ASTRONOMY & ASTROPHYSICS
SUPPLEMENT SERIES

Astron. Astrophys. Suppl. Ser. **130**, 333–339 (1998)

Kinematics of the local universe

VII. New 21-cm line measurements of 2112 galaxies⋆,⋆⋆

G. Theureau[1], L. Bottinelli[1,3], N. Coudreau-Durand[1], L. Gouguenheim[1,3], N. Hallet[1], M. Loulergue[1], G. Paturel[4], and P. Teerikorpi[2]

[1] Observatoire de Paris/Meudon, ARPEGES/CNRS URA1757, F-92195 Meudon Principal Cedex, France
[2] Tuorla Observatory, 21500 Piikkiö, Finland
[3] Université Paris-Sud, F-91405 Orsay, France
[4] Observatoire de Lyon, F-69561 Saint-Genis Laval Cedex, France

Received November 28; accepted December 24, 1997

Abstract. This paper presents 2112 new 21-cm neutral hydrogen line measurements carried out with the meridian transit Nançay radiotelescope. Among these data we give also 213 new radial velocities which complement those listed in three previous papers of this series. These new measurements, together with the HI data collected in LEDA, put to 6 700 the number of galaxies with 21-cm line width, radial velocity, and apparent diameter in the so-called KLUN sample.

Key words: catalogs — galaxies: distances and redshifts; ISM — radio lines: galaxies

1. Introduction

The present paper is the fourth in a series (I: Bottinelli et al. 1992; II: Bottinelli et al. 1993; III: di Nella et al. 1996) which intends to complement optical catalogues with new radial velocity, 21-cm line width, and HI-flux measurements. Our aim was to build a large sample of spiral galaxies, complete down to a photometric diameter of 1.6 arcmin, and having unbiased Tully-Fisher distances. First applications of this KLUN programme, dedicated to the study of the Kinematics of the Local UNiverse, started in 1990 (Paturel et al. 1990) and cover several topics of discussion on:

- the completeness of the sample (Paturel et al. 1994)
- the homogenization of optical and radio data in connexion with the Lyon-Meudon Extragalactic database LEDA (Bottinelli et al. 1990)
- the effect of disc opaqueness on observed optical B-band parameters (Bottinelli et al. 1995)
- the dependence of the TF relation on morphological type and mean surface brightness and the improvement of this distance indicator (Theureau et al. 1997a; Theureau 1998)
- the determination of the Hubble constant H_0 from TF B-band and $\log D_{25}$ relations (Theureau et al. 1997b).

We present here the result of our Nançay HI-survey, in the period between 1988 and 1996, from a catalogue of 2711 spiral galaxies (from Sa to Sdm). In addition to the 664 previously published (Papers I and II) radial velocities, we give 213 new velocity measurements, and 21-cm line widths and HI fluxes for 2112 objects of the observed sample, together with their 21-cm line profile, signal to noise ratio S, and rms noise $\sigma_{\rm ext}$. These new observations put to 6700 the number of spiral galaxies contained in our KLUN sample.

The Nançay radiotelescope and processing chain are briefly presented in Sect. 2. The actual detection rate is discussed in Sect. 3, and the data processing in Sects. 4, 5, and 6. Finally, Sect. 7 presents our conclusions on observational errors and completeness of the HI-sample.

2. Observations

The totality of these observations has been carried out with the meridian-transit Nançay radiotelescope (France). This instrument is a single dish antenna with a collecting area of 6912 m^2 (200 × 34.56) equivalent to that of a 94 m-diameter parabolic dish. The half-power beam width at

Send offprint requests to: theureau@obspm.fr

⋆ Figure 5 and Appendices A and B for corresponding comments are available in electronic form at the http://www.edpsciences.com

⋆⋆ Table 2 is only available in electronic form at the CDS via anonymous ftp to cdsarc.u-strasbg.fr (130.79.128.5) or via http://cdsweb.u-strasbg.fr/Abstract.html

21-cm is 3.6 arcmin (EW) × 22 arcmin (NS) (at zero declination). The minimal system temperature at $\delta = 15°$ is about 37 K in both horizontal and vertical polarizations. The spectrometer is a 1024-channel autocorrelator of 6.4 MHz bandwidth. The spacing of the channels corresponds to 2.6 km s^{-1} at 21 cm with a bank of 512 channels in each polarization. After boxcar smoothing the final resolution is typically 10 km s^{-1}. In the velocity-search mode the 1024 channels are split in four banks of 256 channels leading to a range of 4800 km s^{-1} (generally from 400 to 5200 km s^{-1} or from 5200 to 10000 km s^{-1}). The gain of the antenna has been calibrated according to Fouqué et al. 1990; the final HI-fluxes (Table 2) are expressed by using as reference a set of 9 calibrator galaxies regularly observed since 1988 (see Sect. 6).

We used the Nançay processing package SIR (Système Interactif de Réduction). The processing chain consists of a selection of good observation cycles (one "observation" is a series of on/off observational sequences), the straightening of the base-line by a polynomial fit, and the application of a boxcar smoothing. The maximum of the line is determined by eye as the mean value of the maxima of each profile's horn after taking into account the medium noise (evaluated in the base-line). The widths, measured at the standard levels 20% and 50% of that maximum, correspond to the "distance" separating the two external points of the profile at these intensity levels.

The total list of corrected HI-astrophysical parameters (Table 2), 21-cm line profiles (Fig. 5), and their corresponding comments (Appendix A and B), is only available in electronic form at the CDS via anonymous ftp to cdsarc.u-strasbg.fr (130.79.128.5) or via http://cdsweb.u-strasbg.fr/Abstract.html or via http://www.edpsciences.com. As an example, the first page of Table 2 and Fig. 5 are presented at the end of this paper.

3. HI detection rate

The investigation of the HI line detection rate is of great interest with regard to the HI-completeness of Tully-Fisher catalogues. In particular, this HI-completeness is required to insure against biases by using the inverse relation ($\log V_{\rm m} = aM + b$; see Ekholm & Teerikorpi 1997), or the TF-21 relation ($M_{\rm HI} = a \log V_{\rm m} + b$, where $M_{\rm HI}$ is the HI mass); note that the latter relies exclusively (except for the inclination of the objects) upon parameters derived from the HI profile of a galaxy (Dole & Theureau 1997).

Concerning the detection rate, it is pertinent to examine separately the observations for which the radial velocity is known from the literature, and those which first require a radio velocity search. 1821 galaxies of our programme (hereafter Sample I) had already a published radial velocity, and 1572 of these have been successfully observed at Nançay. This proportion corresponds to a mean detection rate of 86.3% (In fact, almost 90% if confused profile due to close companions are taken into account). In the same way, for the velocity search mode which concerned 890 objects (hereafter Sample II), we got 540 new velocities and HI profiles, corresponding to a mean detection rate of 61%.

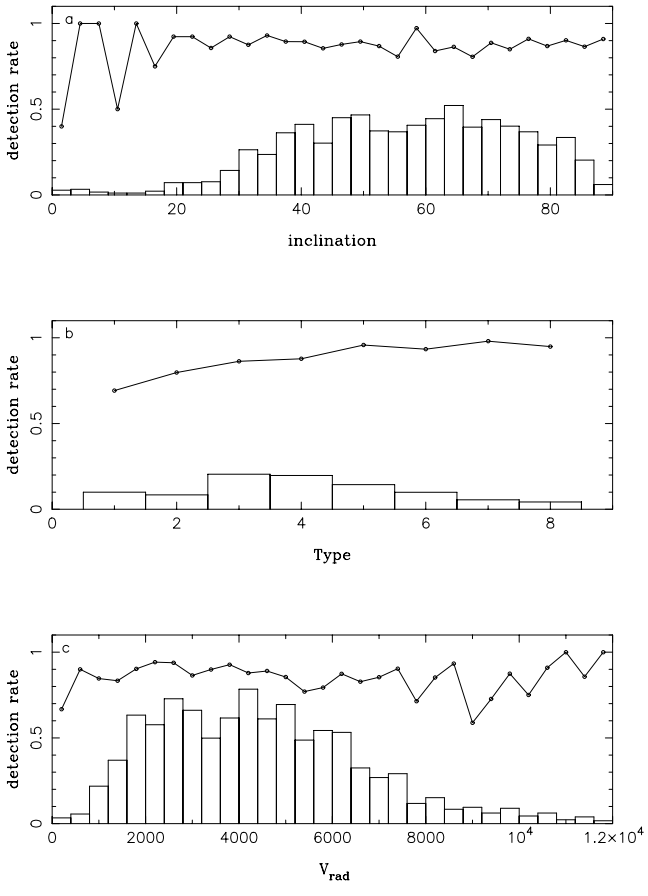

Fig. 1. detection rate as a function of: **a)** inclination, **b)** Type, **c)** radial velocity, for galaxies of known velocity

However, it is important to make a more detailed study: we could suspect, for example, that very inclined objects (edge-on spirals), which have generally a rather wide profile for a low signal to noise ratio, are less easily detectable than face-on objects. Early type spirals, which contain less neutral hydrogen gas than late type spirals, are also expected to be less detectable. Finally, for galaxies having a known radial velocity, it is interesting to study the detection rate with increasing redshift. Figures 1a (resp. 2a), 1b (resp. 2b), and 1c show the detection rate (broken line) respectively as a function of inclination, morphological type, and radial velocity for Sample I (resp. Sample II). The histogram on the bottom of each panel represents the ratio of the number of objects relative to the total sample size (samples I or II). For this ratio $n/n_{\rm tot}$, in Figs. 1a, 1c, and 2a, the scale of the actual vertical axis must be divided by 10.

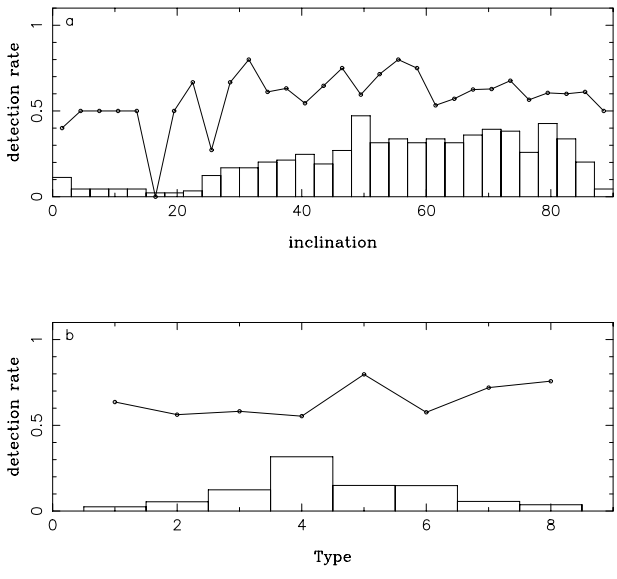

Fig. 2. detection rate as a function of: **a)** inclination, **b)** Type, for galaxies in velocity search mode

Note the following conclusions: (i) there is no special dependence against inclination, (ii) there is as expected a slight significant increase of the detection rate from early to late types ($\simeq$ 15%, well seen in Fig. 1b), and (iii) no clear decrease can be observed against the distance (at most 5% between $v = 0$ and $v = 6000$ km s^{-1}). These results are promising for Tully-Fisher applications.

4. Radial velocities

Our observed radial velocities are listed in Table 2 (Col. 5) and correspond to the median point of the 21-cm line profile measured at 20% level of maximum intensity. 540 of these measurements have been made in velocity search mode (see Fouqué et al. 1990); part of them has been already published in two previous papers (Bottinelli et al. 1992, 1993). For the other 1572 velocities, we have used the existing published data to "sight" directly the appropriate frequency band.

The internal mean error on V_{20} is calculated according to Fouqué et al. 1990 as follows:

$$\sigma(V_{20}) = \frac{4 \cdot (R \cdot \alpha)^{1/2}}{S/N}$$

where R is the actual spectral resolution, $\alpha = (W_{20} - W_{50})/2$ is the slope of the line profile, and S/N is the signal to noise ratio. The average of $\sigma(V_{20})$ is about 8 km s^{-1}.

5. Line widths and log $V_{\rm m}$

Line widths are measured on the observed profile at two standard levels corresponding to 20% and 50% of the maximum intensity of the line. The results listed in Table 2 (Cols. 7 and 9) have been corrected to the optical velocity scale. According to Fouqué et al. (1990), the mean measurement error is equal to $3 \cdot \sigma(V_{20})$ and $2 \cdot \sigma(V_{20})$ for the 20% and 50% widths, respectively. We give in column 11 the derived value of the logarithm of the maximum of circular velocity $\log V_{\rm m}$. It has been calculated as follows. The widths W_{20} and W_{50} are first corrected for resolution effect:

$$W_{l,R=0} = W_{l,R} + (0.014 \cdot l - 0.83)$$

for $l = 20$ and $l = 50$ (Bottinelli et al. 1990), and further corrected for internal velocity dispersion:

$$W_{\rm c} = W^2 + w_{\rm t}^2(1 - 2{\rm e}^{-W_{\rm s}^2/w_{\rm r}^2}) - 2W \cdot w_{\rm t}(1 - {\rm e}^{-W_{\rm s}^2/w_{\rm r}^2})$$

where $w_{\rm t} = 2\sigma_{\rm z} \cdot k(l)$, assuming an isotropic distribution of the non-circular motions $\sigma_{\rm z} = 12$ km s^{-1} and a nearly Gaussian velocity distribution ($k(20)$=1.96 and $k(50)$=1.13; Fouqué et al. 1990).

Corrected W_{20} and W_{50} are finally used to calculate $\log V_{\rm m}$:

$$\log V_{\rm m} = (2 \log W_{20} + \log W_{50})/3 - \log(2 \sin {\it incl}).$$

Where the inclination *incl* is derived from:

$$\sin^2({\it incl}) = \frac{1 - 10^{2 \log R_{25}}}{1 - 10^{2 \log r_0}}$$

R_{25} is the axis ratio and $\log r_0 = 0.43 + 0.053T$ for type T= 1 to 7 and $\log r_0$=0.38 for T=8. The actual uncertainty on $\log V_{\rm m}$ has been calculated according to Bottinelli et al. 1983. 94% of our observations have a signal to noise ratio S/N greater than 3; 62% have a signal to noise ratio greater than 5. Figure 3 shows the observed line widths as a function of S/N.

For information, the above corrections for resolution effect and non-circular motions represent on average about 18% and 11% of the observed line width, for the 20% and 50% level respectively. They lead to a correction of $\sim$3.3% on average on $\log V_{\rm m}$.

6. HI-fluxes

HI-fluxes $F_{\rm HI}$ (Table 2, Col. 13) are expressed in Jy km s^{-1} and corrected for beam-filling according to Bottinelli et al. (1990):

$$F_{\rm HI} = R \cdot F$$

where F is the observed raw HI-flux,

$$R = \left[1 + \frac{D_{25}^2 \sin^2\beta + d_{25}^2 \cos^2\beta}{22}\right]^{\frac{1}{2}}$$

and β is the position angle of the galaxy defined northeastwards, D_{25} and d_{25} are the photometric major and minor axis respectively.

These fluxes have been first calibrated according to a set of close calibrating galaxies, whose HI-fluxes F_0 (see Table 1) were accurately measured by Fouqué (1982) and which have been regularly observed (once a month each on average) during all the period covered by our programme.

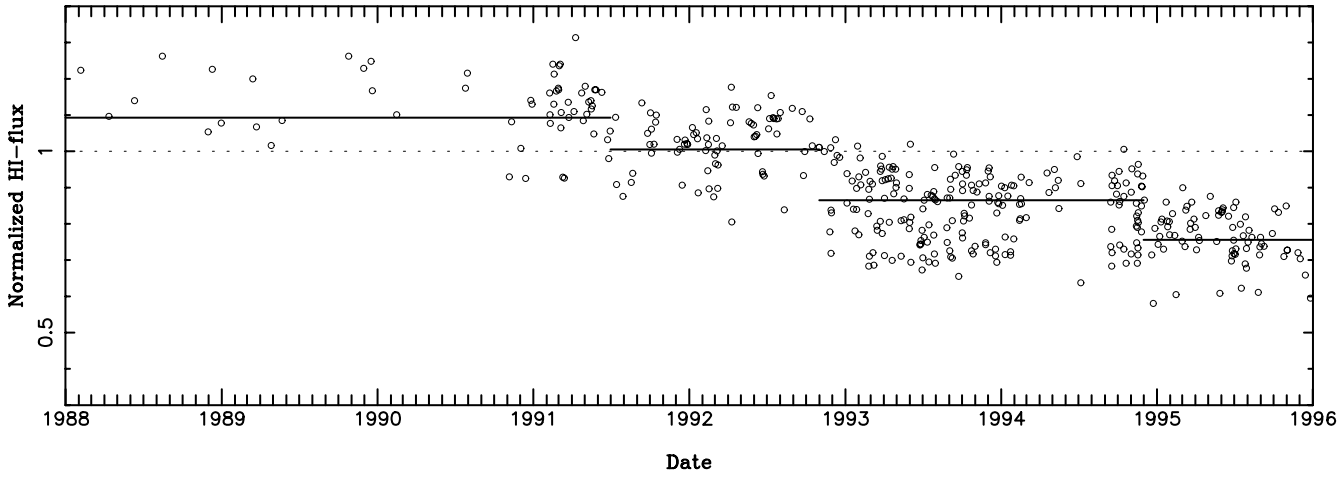

Fig. 4. Evolution of the HI-flux ($F_{\rm HI}/F_0$) of our 9 calibrating galaxies during the HI survey

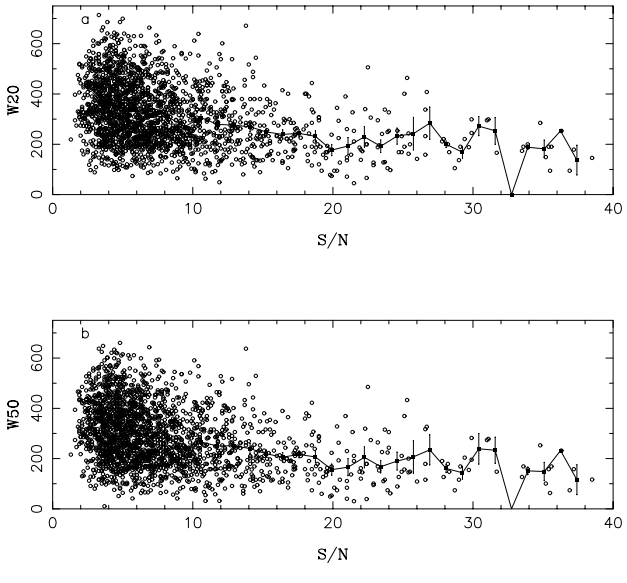

Fig. 3. observed line width, **a)** W_{20} and **b)** W_{50}, as a function of signal to noise ratio S/N

Table 1. Calibrating galaxies

Name	R.A. (1950) DEC.	T	F_0 Jy km s^{-1}
NGC 1058	02 40 23 +37 07 48	5	44.88
NGC 1518	04 04 38 −21 18 44	8	50.66
NGC 1637	04 38 57 −02 57 11	5	38.43
NGC 2344	07 08 46 +47 15 02	5	16.68
NGC 5477	14 03 48 +54 42 02	9	21.27
NGC 6384	17 29 59 +07 05 43	4	49.00
NGC 6814	19 39 55 −10 26 37	4	21.03
NGC 7292	22 26 06 +30 02 09	10	16.63
IC 2233	08 10 28 +45 53 43	7	43.85

Column 1: galaxy name
Column 2: right ascension and declination (1950)
Column 3: morphological type
Column 4: HI-flux from Fouqué (1982).

The evolution of the ratio $F_{\rm HI}/F_0$ with time allows us to supervise the Nançay system and to get for each observation the optimal flux measurement. We have exhibited four main periods of gain stability separated by ponctual steps which can be related to a change of either a diode or a cable along the acquisition chain (Fig. 4).

7. Conclusion: Observational errors and selection effects

The mean error of the $\log V_{\rm m}$ determinations are in most of the cases better than 0.1, and the HI-fluxes, in terms of external errors, can be considered as correct within $\simeq$15% of uncertainty at the 2-σ level. Errors on radial velocities are generally smaller than 20 km s^{-1}, the mean error over the whole sample being about 8 km s^{-1}.

Part of the observed HI-profiles given in Fig. 5 were recognized as confused, because one or several other galaxies are within the beam. These objects are marked with an "a" or a "c" in the last column of Table 2, and individual comments, mainly about possible companions or data quality, may be found in Appendix A; references related to these comments are listed in Appendix B.

Considering possible selection effects, no dependence of the detection rate on inclination, line width, or distance, were observed in the investigated redshift range ($V \leq 10\,000$ km s^{-1}). However, the 10 percents of missing objects (i.e. unsuccessfully observed) indicates a possible cut-off of the $\log V_{\rm m}$ distribution. It is indeed probable that, due to noise fluctuations or base-line effects, one tends to miss very narrow as well as very wide HI-profiles. This means that one has to be careful when determining for example the Hubble constant H_0 from the inverse Tully-Fisher relation, because a systematic effect, comparable to the Malmquist bias in the direct case, is expected. This debate is presented in details by Ekholm & Teerikorpi (1997), and will be further discussed in a forthcoming paper.

It has been shown also that the HI detection rate is slightly correlated with morphological type. This (expected) result implies that it is necessary to process separately the different types when using either the inverse TF relation, or the TF-21 relation (relation between the 21-cm magnitude and $\log V_{\rm m}$).

Acknowledgements. We have made use of data from the Lyon-Meudon Extragalactic Database (LEDA) compiled by the LEDA team at the CRAL-Observatoire de Lyon (France).

References

Bottinelli L., Gouguenheim L., Paturel G., Vaucouleurs G. de, 1983, A&A 118, 4
Bottinelli L., Gouguenheim L., Fouqué P., Paturel G., 1990, A&AS 82, 391
Bottinelli L., Durand N., Fouqué P., et al., 1992, A&AS 93, 173 (Paper I)
BottinelliL., Durand N., Fouqué P., et al., 1993, A&AS 102, 57 (Paper II)
Bottinelli L., Gouguenheim L., Paturel G., Teerikorpi P., 1995, A&A 296, 64
Dole H., Theureau G., 1997, C.R. Acad. Sci. Paris, t. 324, Ser. IIb, p. 201-208
Ekholm T., Teerikorpi P., 1997, A&A 325, 33
Fouqué P., 1982, PhD Thesis, University of Paris
Fouqué P., Bottinelli L., Gouguenheim L., Paturel G., 1990, ApJ 349, 1
di Nella H., Paturel G., Walsh A.J., et al., 1996, A&ASP 118, 311 (Paper III)
Paturel G., Fouqué P., Bottinelli L., Gouguenheim L., 1989, A&AS 80, 299
Paturel G., Bottinelli L., Fouqué P., Gouguenheim L., Teerikorpi P., 1990, The Messenger 62, 8
Paturel G., Bottinelli L., Di Nella H., et al., 1994, A&A 289, 711
Theureau G., Hanski M., Teerikorpi P., et al., 1997a, A&A 319, 435
Theureau G., Hanski, Ekholm T., et al., 1997b, A&A 322, 730
Theureau G., 1998, A&A 331, 1

Table 2. -excerpt. Astrophysical HI-parameters

PGC/LEDA NAME	R.A.(1950)	DEC.(1950)	V20	rms	W20	rms	W50	rms	logVm	rms	F_HI	rms	S/N	Note
(1) (2)	(3)	(4)	(5)	(6)	(7)	(8)	(9)	(10)	(11)	(12)	(13)	(14)	(15)	(16)
PGC 00012 MCG -1- 1-16	23 57 34	-06 39 11	6547	8	410	25	399	17	2.262	.027	3.7	.9	4.8	
PGC 00070 UGC 12900	23 58 24	20 04 00	6796	8	446	24	429	16	2.301	.024	5.6	1.0	5.8	
PGC 00073 ESO 349-17	23 58 24	-33 53 24	6898	11	175	33	153	22	2.094	.099	2.9	.9	4.8	
PGC 00102 IC 5376	23 58 46	34 14 51	5032	4	425	13	416	9	2.281	.014	5.3	.8	8.6	II
PGC 00176 MCG -1- 1-24	00 00 01	-03 59 20	6468	10	365	29	342	19	2.297	.036	3.3	.7	5.4	
PGC 00186 UGC 3	00 00 11	18 37 00	7888	7	481	22	464	15	2.396	.020	4.6	.7	6.4	II
PGC 00195 NGC 7812	00 00 21	-34 30 48	6806	12	236	37	224	24	2.099	.076	3.1	1.1	3.4	
PGC 00205 UGC 5	00 00 32	-02 11 29	7271	6	461	19	459	12	2.376	.018	5.3	1.2	4.3	
PGC 00250 UGC 14	00 01 01	22 55 19	7237	9	351	26	331	18	2.258	.035	4.7	1.0	5.7	
PGC 00305 UGC 27	00 01 54	05 34 00	3114	4	232	13	219	9	2.060	.028	10.4	1.5	9.8	
PGC 00366 UGC 36	00 02 40	06 29 34	6351											c
PGC 00393 UGC 39	00 03 00	53 22 00	9523	7	519	22	496	15	2.422	.019	4.0	.5	7.0	
PGC 00515 UGC 52	00 04 15	08 21 04	5284	9	318	28	216	18	9.999	9.999	6.7	.6	11.3	
PGC 00540 UGC 55	00 04 24	46 23 00	5138	11	131	32	122	22	1.876	.130	2.4	1.1	3.5	
PGC 00558 ESO 538-22	00 04 37	-22 03 54	10181	18	538	53	510	35	2.388	.043	2.5	.8	3.3	
PGC 00627 NGC 7	00 05 48	-30 11 36	1495	2	184	7	156	5	1.839	.020	13.5	.8	25.1	
PGC 00634 NGC 10	00 06 02	-34 08 12	6803	16	600	49	557	33	2.482	.036	5.5	1.3	4.2	
PGC 00638 UGC 71	00 06 00	43 49 06	8162	38	335	113	243	75	2.198	.172	1.3	.6	2.6	
PGC 00659 ESO 349-33	00 06 32	-33 11 36	6890	9	460	28	452	19	2.319	.027	4.0	.9	3.9	
PGC 00767 NGC 29	00 08 12	33 04 24	4762	10	393	29	354	20	2.276	.034	6.1	1.2	6.8	
PGC 00798 NGC 36	00 08 48	06 06 42	6030	4	449	13	430	9	2.395	.013	7.8	.9	11.0	
PGC 00878 UGC 119	00 10 28	14 07 58	2023	4	142	12	83	8	1.752	.050	6.2	.6	21.0	I
PGC 00913 UGC 128	00 11 12	35 43 00	4531	4	228	12	212	8	2.194	.026	7.7	1.0	11.7	
PGC 00963 UGC 139	00 11 55	-01 01 23	3963	4	311	12	292	8	2.164	.017	13.1	1.3	12.8	
PGC 00967 NGC 47	00 11 56	-07 27 00	5700	3	211	10	200	7	9.999	9.999	4.6	.7	11.6	
PGC 00978 NGC 52	00 12 06	18 18 12	5407	12	543	35	527	24	2.396	.028	2.7	.7	4.0	II
PGC 00983 NGC 50	00 12 11	-07 37 25	5701	9	226	28	220	19	9.999	9.999	2.4	.9	3.6	
PGC 01099 UGC 153	00 14 00	47 40 00	4385	15	241	46	204	30	1.977	.096	6.2	1.6	4.3	
PGC 01109 MCG -1- 1- 64	00 14 18	-05 33 00	3958	10	303	30	266	20	2.097	.047	4.9	.9	6.6	
PGC 01130 ESO 539-5	00 14 38	-19 34 42	3203	6	263	17	258	12	2.130	.031	2.7	.6	5.5	
PGC 01198 UGC 171	00 15 44	48 27 11	5268	13	346	40	324	27	2.296	.054	5.3	1.4	3.9	
PGC 01211 NGC 73	00 16 06	-15 36 00	7762	10	526	31	466	21	2.482	.026	4.5	.6	7.8	II
PGC 01414 MCG 8- 1-41	00 19 20	48 51 22	5143	9	248	26	246	17	9.999	9.999	999.9	99.9	3.1	
PGC 01419 MCG -1- 2- 6	00 19 36	-04 37 27	4353	8	193	23	189	15	2.060	.060	2.3	.8	3.9	
PGC 01518 NGC 101	00 21 25	-32 48 48	3383	4	185	13	170	8	2.038	.035	13.0	1.6	10.7	
PGC 01547 MCG -1- 2-10	00 22 06	-06 19 00	8182	12	323	35	306	23	2.218	.050	2.4	.7	4.1	
PGC 01572 UGC 238	00 22 26	31 04 04	6796	13	469	39	392	26	2.307	.039	6.2	1.1	6.9	
PGC 01577 UGC 240	00 22 37	06 13 00	8657	24	388	71	320	47	2.239	.087	3.3	1.2	3.6	II
PGC 01591 UGC 242	00 22 52	19 57 39	4405	6	303	19	276	12	2.324	.029	5.5	.7	9.2	*
PGC 01592 UGC 243	00 22 48	45 38 42	5073	22	623	67	555	45	2.447	.048	4.0	.9	3.8	II
PGC 01609 MCG -1-2-11	00 23 15	-02 33 41	5339	6	429	17	401	12	2.278	.018	9.2	1.1	10.0	
PGC 01634 MCG -1- 2-14	00 23 44	-04 46 09	3985	8	316	23	290	16	2.127	.035	5.7	.8	7.2	
PGC 01651 MCG 115	00 24 18	-33 57 12	1828	999	205	999	239	999	1.960	9.999	16.2	1.2	18.7	
PGC 01715 NGC 124	00 25 19	-02 05 12	4060	6	271	17	233	11	2.114	.030	8.0	.9	11.8	
PGC 01723 UGC 275	00 25 23	02 14 00	4385	6	231	17	207	12	2.021	.038	3.9	.7	9.3	II
PGC 01736 UGC 279	00 25 37	30 31 33	6298	11	478	34	413	23	2.327	.033	7.2	1.0	7.3	
PGC 01746 UGC 282	00 25 48	03 07 00	4082											c
PGC 01841 MCG -2- 2- 30	00 27 36	-11 23 00	3513	6	335	19	308	13	2.176	.027	5.1	.8	8.8	
PGC 01909 MCG -2- 2- 38	00 28 42	-10 45 00	3589	7	313	20	254	13	2.244	.031	11.7	1.2	12.1	

Column 1: PGC or LEDA galaxy name;
Column 2: most usual galaxy name;
Column 3: right ascension (1950);
Column 4: declination (1950);
Column 5: systemic heliocentric radial velocity (km s^{-1});
Column 6: rms error (km s^{-1});
Column 7: total line width at 20% of the maximum intensity (km s^{-1});
Column 8: rms error (km s^{-1});
Column 9: total line width at 50% of the maximum intensity (km s^{-1});
Column 10: rms error (km s^{-1});
Column 11: logarithm of maximum of rotational velocity;
Column 12: rms error;
Column 13: corrected HI-flux (Jy km s^{-1});
Column 14: rms error (Jy km s^{-1});
Column 15: signal to noise ratio;
Column 16: "c" for HI-confused profile; "a" for HI-confused but measurable profile; "*" when the profile does not appear in Fig. 5; "I" or "II" when the profile was already published in Papers I or II.

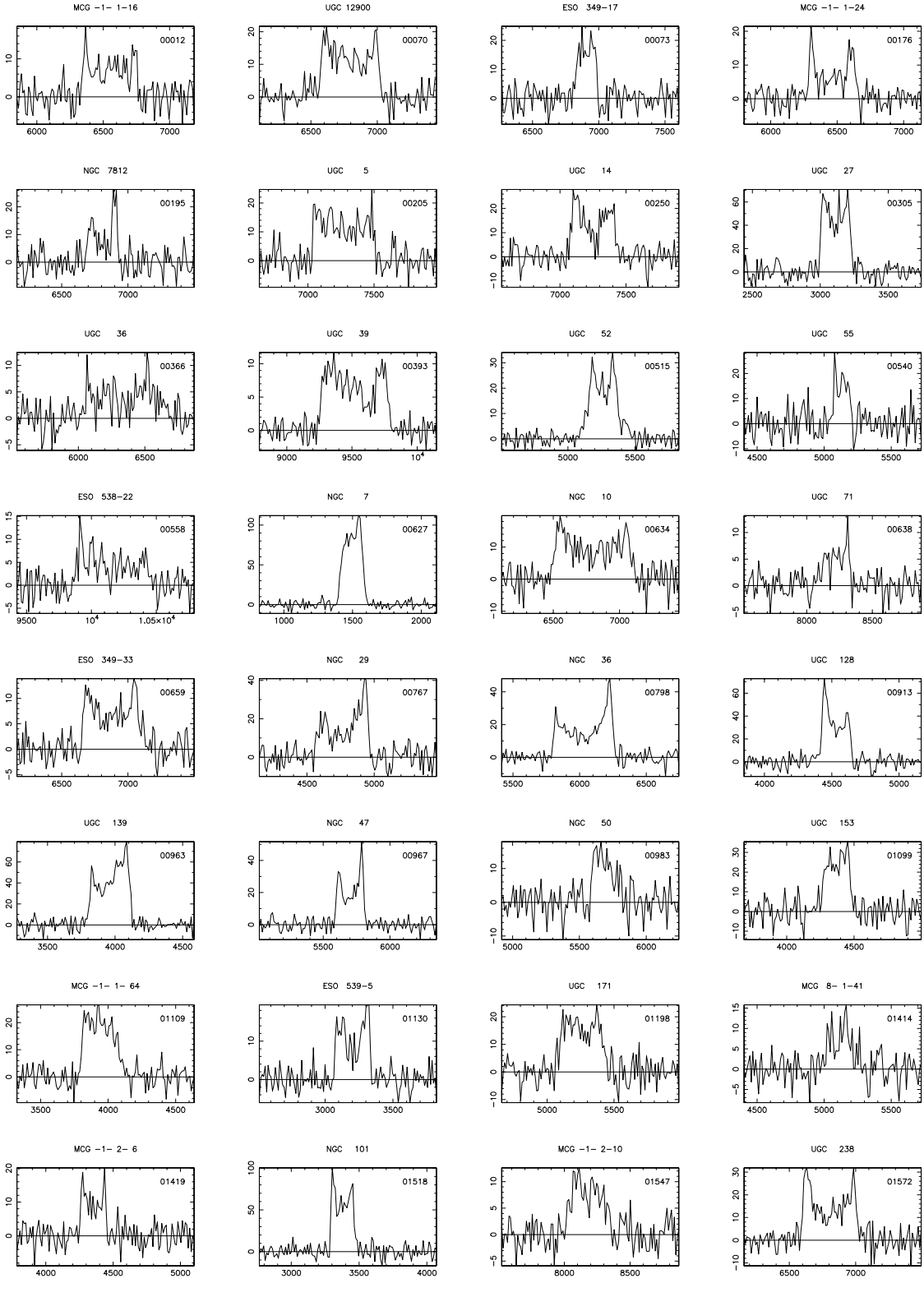

Fig. 5. -excerpt. 21-cm line profiles of galaxies listed in Table 2; profiles are classified according to their PGC name appearing in the top right corner of each panel. The usual name of the galaxy (NGC, UGC, IC, ESO, MCG...) is written above each panel. Ordinate and abscissae axis are graduated respectively in km s^{-1} and mJy. Note that heliocentric radial velocities are expressed in terms of optical redshift $c\frac{\Delta\lambda}{\lambda}$. The horizontal line represents the baseline of the profile, from which the maximum is estimated